Journal of
Automation and Automobile Engineering

e-ISSN: 2582-3159
Volume-5, Issue-3 (September-December, 2020)

www.matjournals.com

Design and Analysis of Twin-Vertical-Tailed Fixed-Wing Unmanned Aerial Vehicle

Kamal Darlami[1], Aditya Amatya[2], Bikash Kunwar [2], Sanjeeb Poudel [2*], Ujwal Dhakal [2]
[1]Assistance Professor, [2]Graduated students,
Department of Mechanical and Aerospace Engineering, Institute of Engineering (IOE), Pulchowk Campus, Nepal

Correspondence Author: 072bme637sanjeeb@pcampus.edu.np

ABSTRACT

Unmanned Aerial Vehicles possess characteristics that make them suitable for use in multiple areas. This project proposes the design of a small fixed-wing UAV that can be used to carry a payload of around 1 kg. The design is developed performing aerodynamic, structural, and stability analysis using analytical methods as well as commercial code. It is then fabricated into a physical model. Take-off is achieved by launching with the hand or a launcher. Low stall speed allows the UAV to land softly during landing. Twin vertical stabilizers are used, one at each end of the horizontal stabilizer, to reduce the effect of propeller slipstream. Pusher configuration is chosen to allow unobstructed view when imaging devices are attached to the nose of the UAV.

Keywords-- UAV, Airfoil, Structural analysis, ANSYS, XFLR5, and Stability

INTRODUCATION

The earliest use of unmanned aerial vehicles (UAVs) was made in the military in the mid-nineteenth century. However, the concept of remotely piloted UAVs is relatively new. It was conceived in the late 1970s, and it was in the mid-1980s that the first UAVs of such type completed their first official test flights. Since then, the technology has been substantially refined, and improvements have been accomplished; non-military use of UAVs is growing, and the possibilities are endless. The use gained further scale after 2006 when government agencies began using UAVs for disaster relief, border surveillance, and wildfire fighting, while corporations to inspect pipelines and spray pesticides on farms.

UAVs come in various types such as fixed-wing UAV, lighter-than-air UAV, rotary-wing UAV, vertical take-off and landing UAV, tilt-rotor or tilt-wing UAVs, tail-sitter, and thrust reversing UAV.

DESIGN OF MUNAL M-72

Concept of Munal M-72

Munal M-72 is a fixed-wing UAV designed to be launched by hand or a launcher. The following requirements are taken into consideration while designing the UAV.

Table 1: *Design Requirements.*

Wing span	2 m
Endurance	≥30 min
Payload	≥1 kg
Mass	≤3.5 kg

While developing Munal M-72, a number of different configurations were considered. Tractor configuration was the first basic configuration considered. But this configuration was rejected so as to place a camera at the nose of the fuselage.

The other options were either to use means of propulsion on either side of the wing or to use a pusher configuration. Former would increase complexity in fabrication. Moreover, a single propulsive system could be chosen so as to produces enough thrust for small UAVs. Thus, it was decided to select a pusher configuration. In this configuration, twin-tail was chosen to minimize the influence of the propeller slipstream on the aircraft's tail. V- tail configuration will increase complexity in control, while two booms from the wing will increase complexity in fabrication. Thus, it was finally decided to go with the following configuration for Munal M-72.

Page 12-30 © MAT Journals 2020. All Rights Reserved

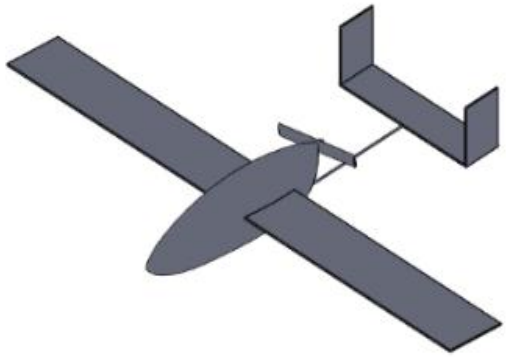

Figure 1: *Final Configuration.*

Airfoil Selection

Different airfoils that are used in UAVs were considered while selecting an airfoil for Munal M-72. Some of the airfoils that are mostly used are listed below,

- Clary Y
- MH 115
- NACA 6411
- Eppler 214
- FALCON

The selection was done by comparing graph between coefficient of lift (C_l), coefficient of drag (C_d) and $\frac{C_l}{C_d}$ for different angle of attack (α). The comparison was done using XFLR5. First, lift and drag coefficient at different angles of attack were calculated using XFLR5 then these points were plotted using MATLAB.

Airfoils characteristics are strongly affected by Reynolds number (Re). Reynolds number defines whether the flow over airfoil will be laminar or turbulent. While comparing, Re of 200,000 was used. This was the approximated Reynolds number while cruising.

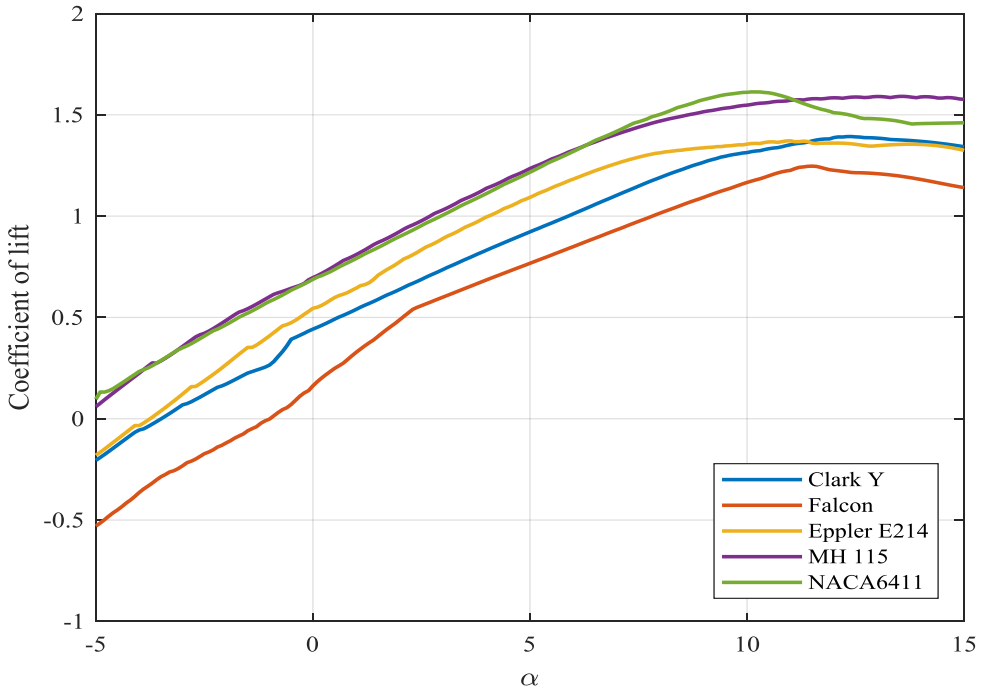

Figure 2: C_l *for Different Airfoils.*

Based on the above comparison, coefficient of lift of NACA 6411 and MH 115 were found to be almost same for different angles of attack. NACA 6411 has maximum lift coefficient and stalls earlier but MH 115 has greater stall angle.

Page 12-30 © MAT Journals 2020. All Rights Reserved

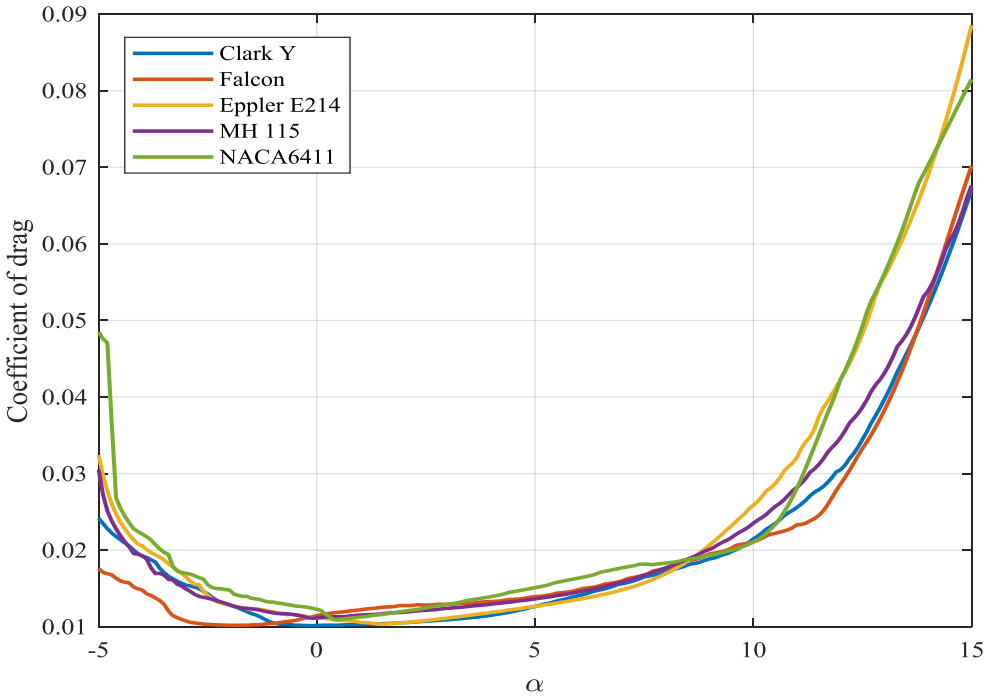

Figure 3: *C_d for Different Airfoils.*

In the figure 3, Clark Y and Eppler E214 have low drag coefficient as compared to others in the range of 0 degree to 8 degrees.

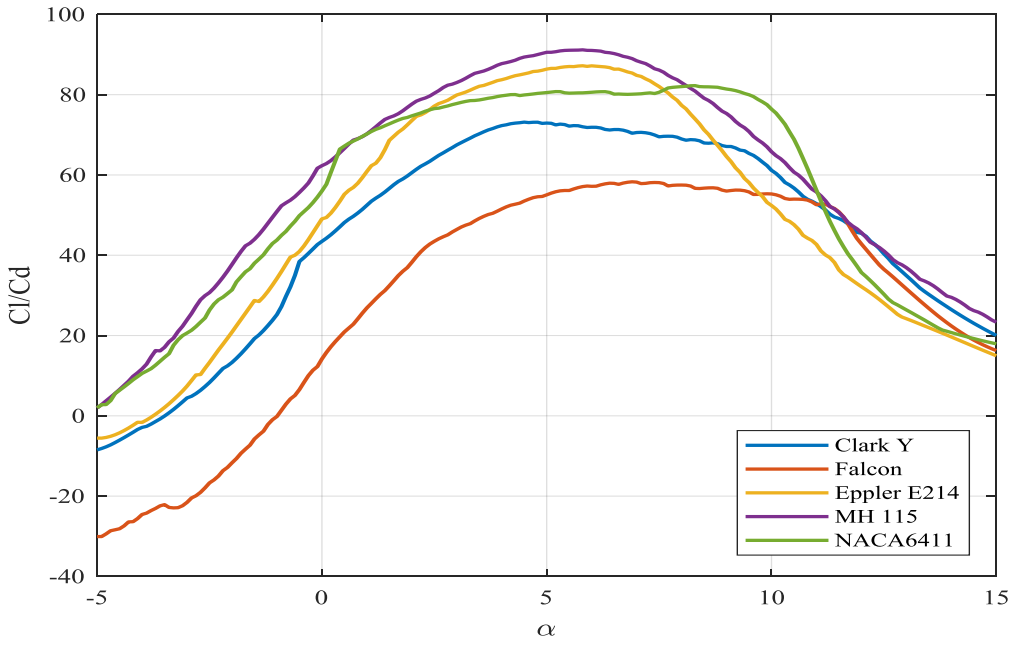

Figure 4: *C_l/C_d for Different Airfoils.*

For almost all angle of attack, coefficient of lift to drag ratio was found to be maximum for MH 115.

In battery powered aircraft, maximum endurance of the aircraft occurs when is $C_L^{\frac{3}{2}}/C_D$ is maximum. Thus, $C_l^{\frac{3}{2}}/C_d$was also compared. Figure 5 shows the graphical comparison between different airfoils.

Page 12-30 © MAT Journals 2020. All Rights Reserved

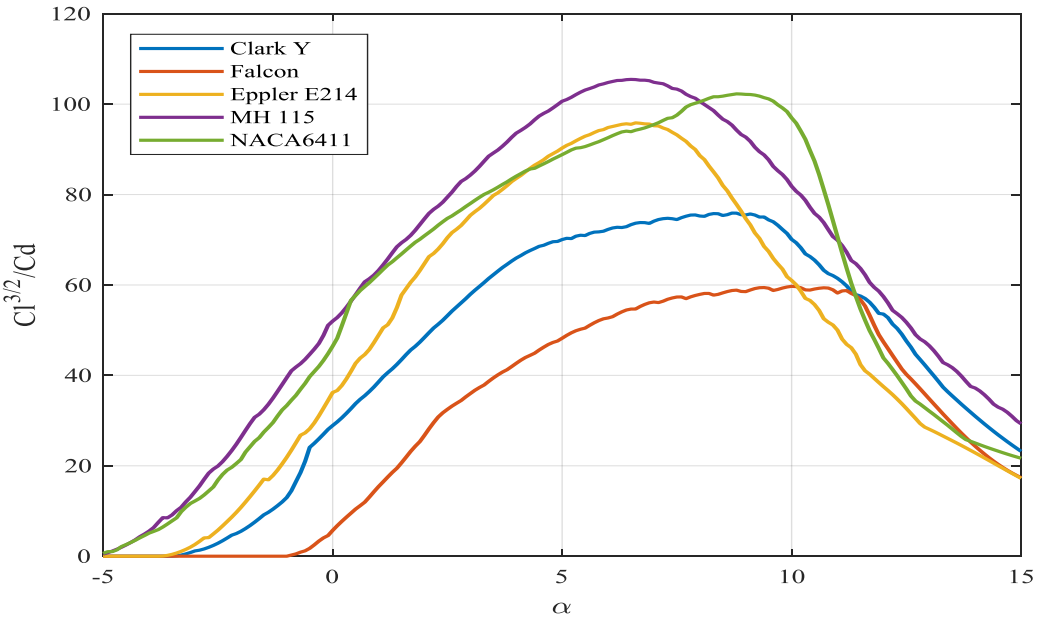

Figure 5: $C_l^{\frac{3}{2}}/C_d$ for different airfoils

$C_l^{\frac{3}{2}}/C_d$ is also maximum for MH115 so, MH 115 was selected for our UAV

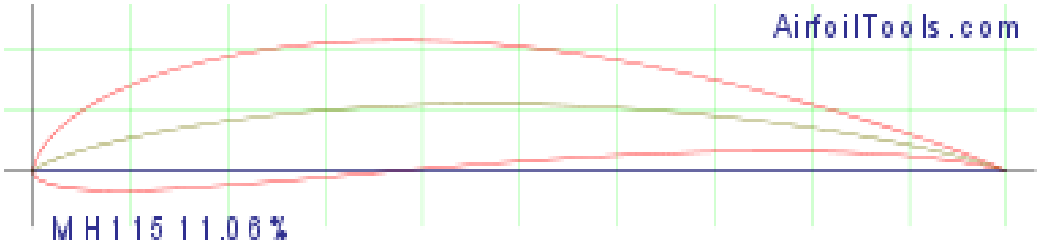

Figure 6: *MH 115*

Table 2: *Geometric Properties of MH 115*

Parameters	**Percentage of chord length**
Maximum Thickness	11.08%
Location of Maximum Thickness	29.29%
Maximum Camber	5.57%
Location of Maximum camber	46.47%

Wing Geometry

For a UAV without landing gear, stall speed as low as practicable is desirable. To have low stall speed, aspect ratio should be low. But low aspect ratio means higher drag force. A MATLAB script was written to see the relationship of aspect ratio with stall speed and induced drag of the wing. For the program, lift curve slope of the wing (C_{Law}) is needed which depends upon the aspect ratio (A) and lift curve slope of the airfoil ($C_{l\alpha}$). In the program, different aspect ratios were defined and C_{Law} for each aspect ratio were calculated using the formula,

$$C_{Law} = \frac{2\pi A}{2 + \sqrt{\left(\frac{2\pi A}{C_{l\alpha}}\right)^2 + 4}}$$

In the above formula, $C_{l\alpha}$ was estimated using graphs given by Pamadi [1], and it was found to be 5.95 rad^{-1}. This value was found very close to the value from XFLR5. Zero-lift angle of attack (α_{0l}) was assumed to be $-5\,degree$. Then, coefficient of lift at the stall angle ($12\,degree$) was calculated. The wing area (S_w) corresponding

Page 12-30 © MAT Journals 2020. All Rights Reserved

to each aspect ratio was calculated using the wing span (b),

$$Sw = \frac{b^2}{A}$$

This area and maximum lift coefficient were used to calculate the stall speed of the wing for a weight of $34.335\,N$. In this analysis, the lift force generated due to empennage and fuselage were ignored.

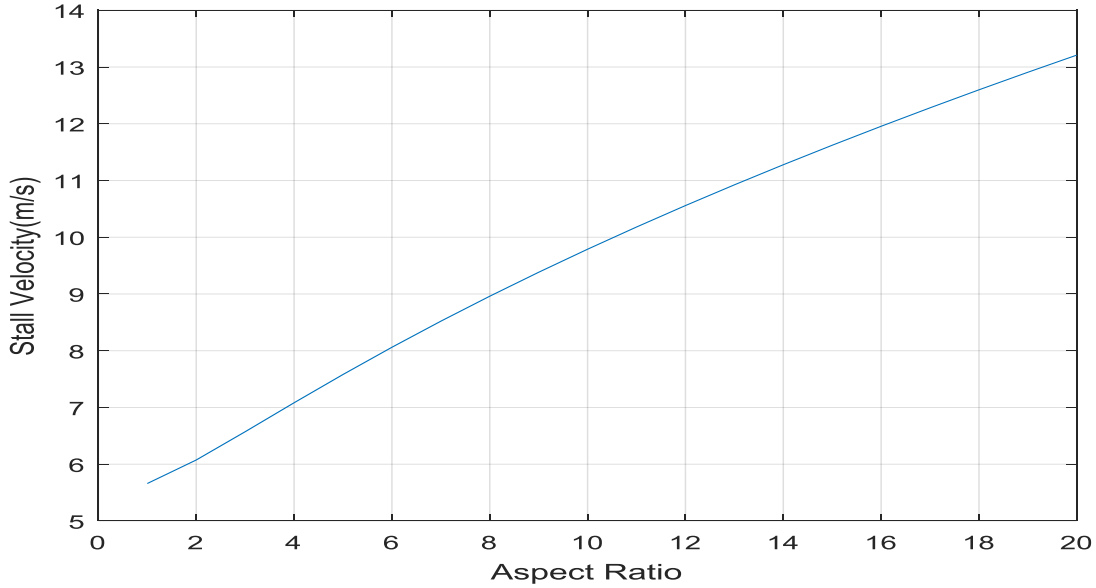

Figure 7: *Stall Velocity For Different Aspect Ratio Of the Wing.*

In the analysis of induced drag and aspect ratio, Oswald efficiency number (e) is required. Oswald efficiency number depends upon aspect ratio, sweep angle and taper ratio. But it was assumed to be 0.85 for all aspect ratio to keep things simple. So, induced drag for alow aspect ratio will be even higher than shown in the figure 8.

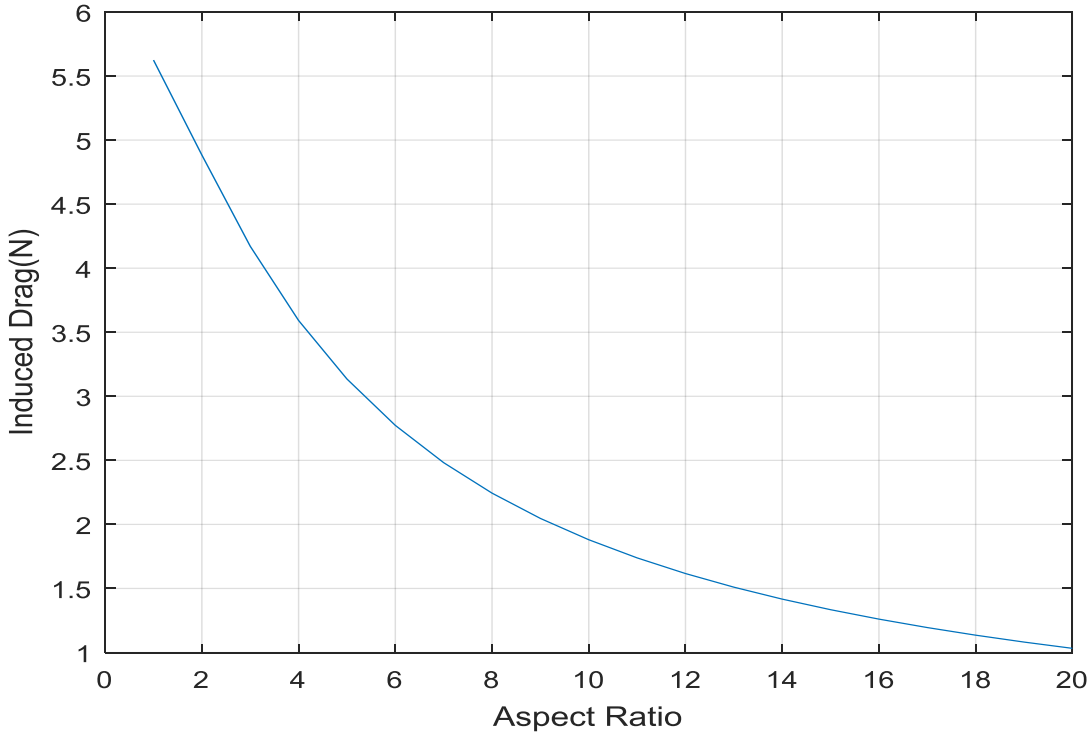

Figure 8: *Induced Drag at Stall For Different Aspect Ratio.*

Page 12-30 © MAT Journals 2020. All Rights Reserved

Increasing aspect ratio increases structural difficulty and problems in fabrication. Thus, it was decided to keep stall speed around 10 m/s and corresponding aspect ratio around 11. By increasing taper ratio, elliptic lift distribution could be approached. But higher taper ratio increases complexity in fabrication. Considering these factors, taper ratio of 0.6 was chosen.

Dihedral increases lateral stability and dihedral angle of 5 $degrees$ was selected. Considering different factors, following wing configuration was selected,

Table 3: *Wing Configuration.*

Span (b)	2 m
Root Chord Length (c_r)	0.225 m
Tip Chord Length (c_t)	0.135 m
Taper ratio (λ)	0.6
Referential Area (S_w)	0.36 m^2
Standard Mean Chord (SMC)	0.180 m
Mean Aerodynamic Chord (MAC)	0.184 m
Aspect Ratio (A)	11.11
Dihedral	5 $degrees$

Above wing was modelled and analyzed using XFLR5. Following graphs show results obtained from the analysis.

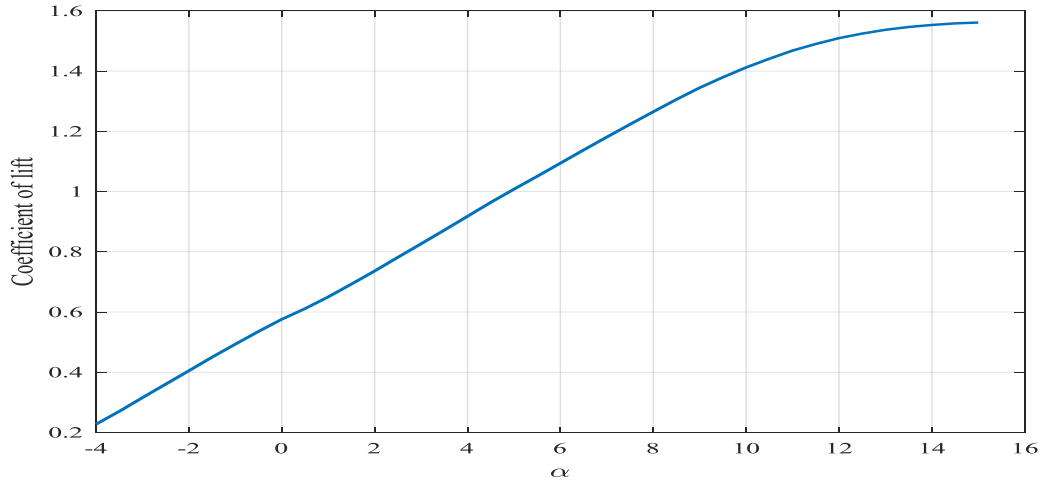

Figure 9: *Variation Of C_L With Angle Of Attack at Constant Lift.*

Figure 9 shows that slope of coefficient of lift ($C_{L\alpha}$) for the wing is 0.088 $degree^{-1}$ and the stall angle is around 15 $degrees$.

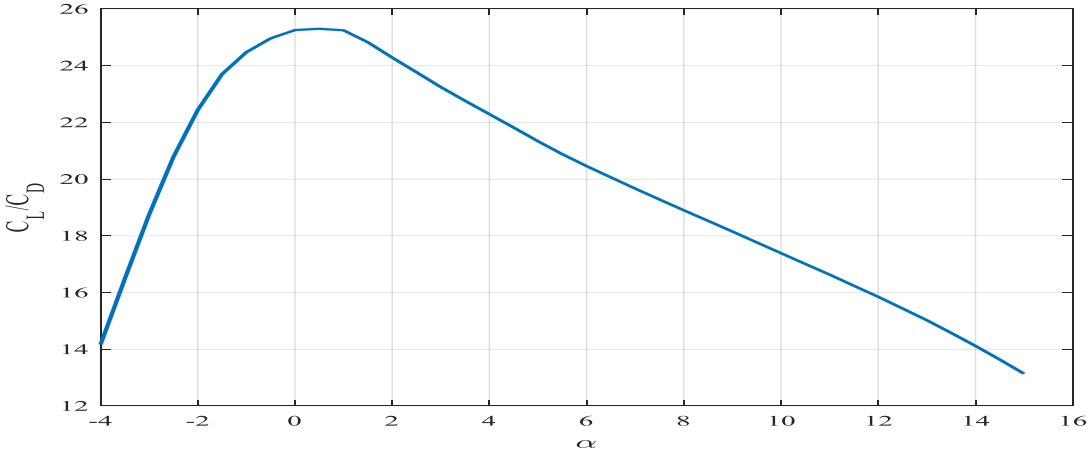

Figure 10: Variation Of C_L/C_D With Angle of Attack at Constant Lift.

Page 12-30 © MAT Journals 2020. All Rights Reserved

For 1 $degree$ angle of attack C_L/C_D is maximum for the wing. Thus, default angle of incidence of the wing (i_w) should be 1 $degree$.

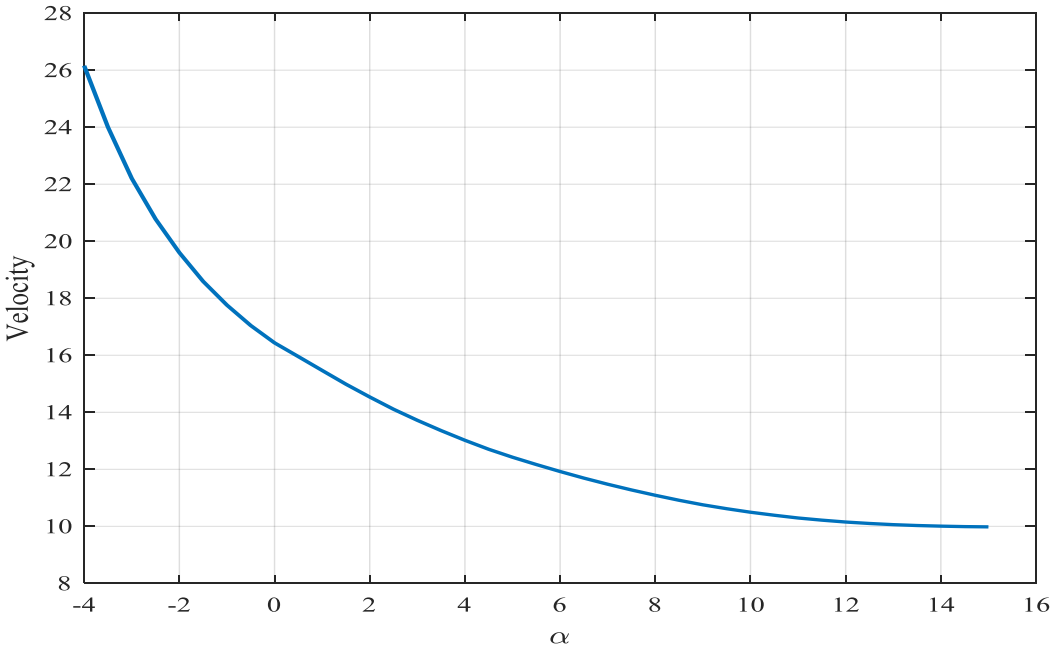

Figure 11: *Variation of Velocity With Angle of Attack.*

Figure 11 shows that the stall velocity of the wing is 10 m/s. This is the minimum velocity at which the wing can generate 34.335 N of lift.

Figure 12 shows orthographic view of the wing in the third angle projection which was modelled in SOLIDWORKS 2016.

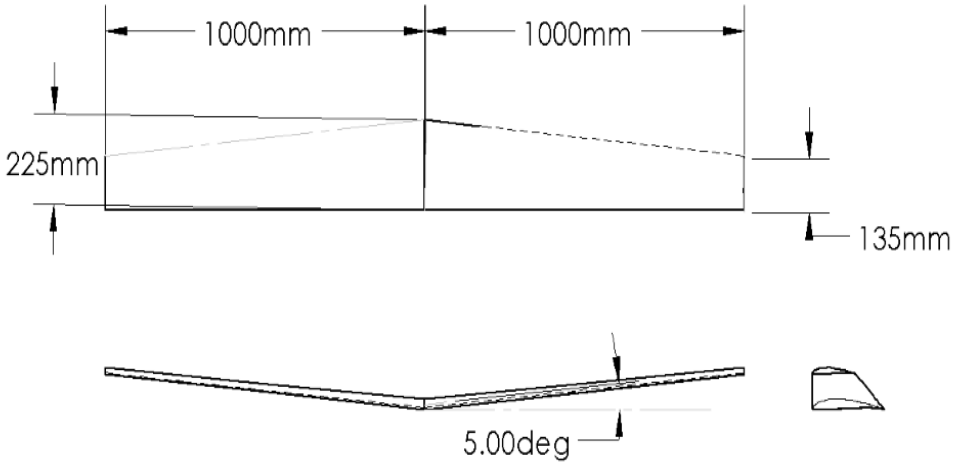

Figure 12: *Orthographic projection of the wing.*

Fuselage Geometry

The fuselage was designed to be spacious in the inside, aerodynamically efficient on the outside, and easier to manufacture. Thus, a rectangular cross section was used. This also meant the payload releasing doors are easier to operate. The edges were filleted with a radius of 20mm so that it will minimize drag under sideslip. The tail of the fuselage was designed so that the propulsion system could be mounted easily and the propeller fits completely with a good amount of clearance with the boom. The nose was designed with a very gradual change in the area, and the overall fuselage was designed to give a good streamlined shape.

Page 12-30 © MAT Journals 2020. All Rights Reserved

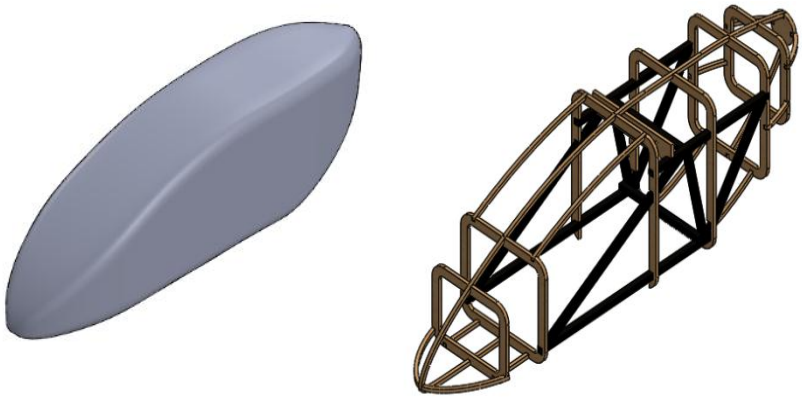

Figure 13: *Fuselage.*

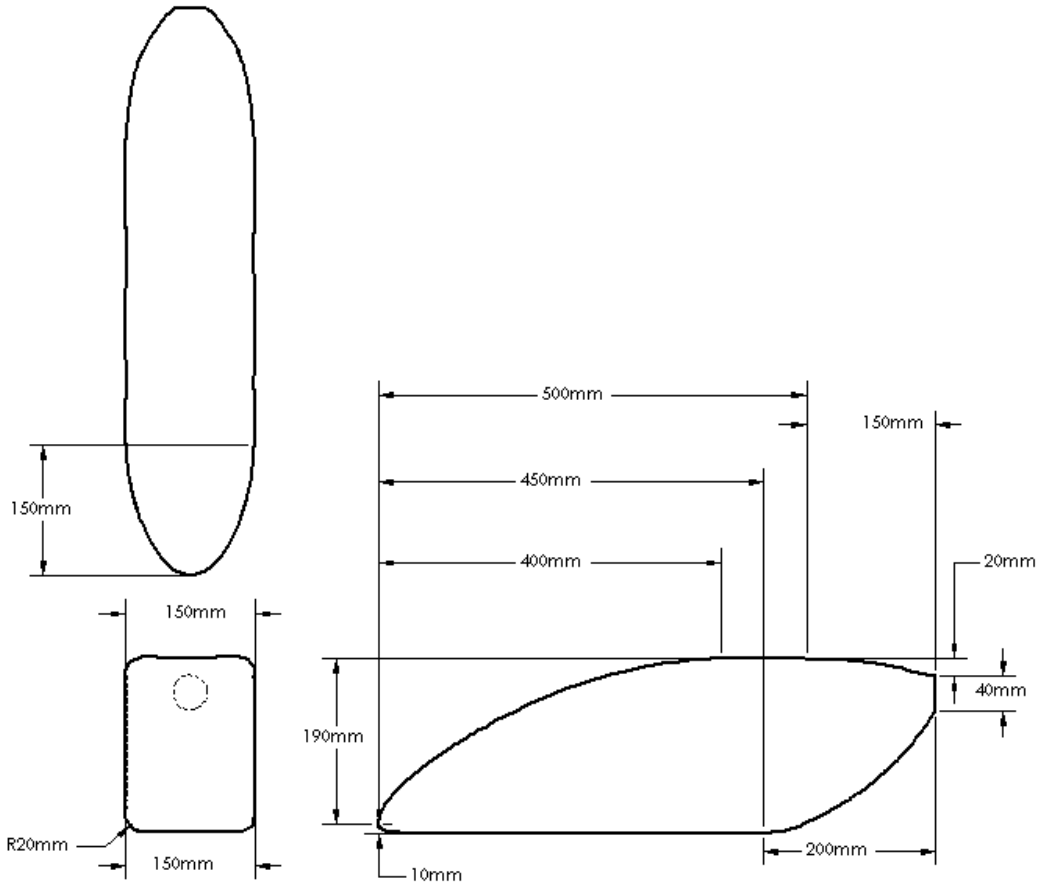

Figure 14: *Orthographic Projection of the Fuselage.*

Empennage Geometry

Symmetric airfoil, NACA 0012, was chosen for the horizontal and vertical stabilizer. It also offered enough thickness for the ease of the fabrication. The empennage was designed to have a single horizontal stabilizer and twin vertical stabilizers. The dimensions of the vertical and horizontal tail planes are determined by using the following equations [2]

$$S_H = \frac{C_{vh} Sc}{l_H}$$

$$S_V = \frac{C_{vv} Sb}{l_V}$$

Tail volume coefficients of 0.5 and 0.04 for horizontal and vertical tails were taken respectively. The following table summarizes the geometry of the empennage.

Page 12-30 © MAT Journals 2020. All Rights Reserved

Table 4: *Empennage sizing*

Parameters	Value
Horizontal tail chord	0.11m
Vertical tail root chord	0.16m
Vertical tail taper ratio	0.6
Individual vertical tail height	0.192m
$L_{[w-t]}$	0.56m
Horizontal tail span	0.415m
Sweep angle for the vertical tail	18.394^0

Aileron geometry

The necessary parameters that define an aileron in relation to the wing are aileron planform area (S_a), aileron chord/wing chord (C_a/C), maximum up and down aileron deflection (δA_{max}), location of inner edge of the aileron along the wing span (b_{ai}) [3].

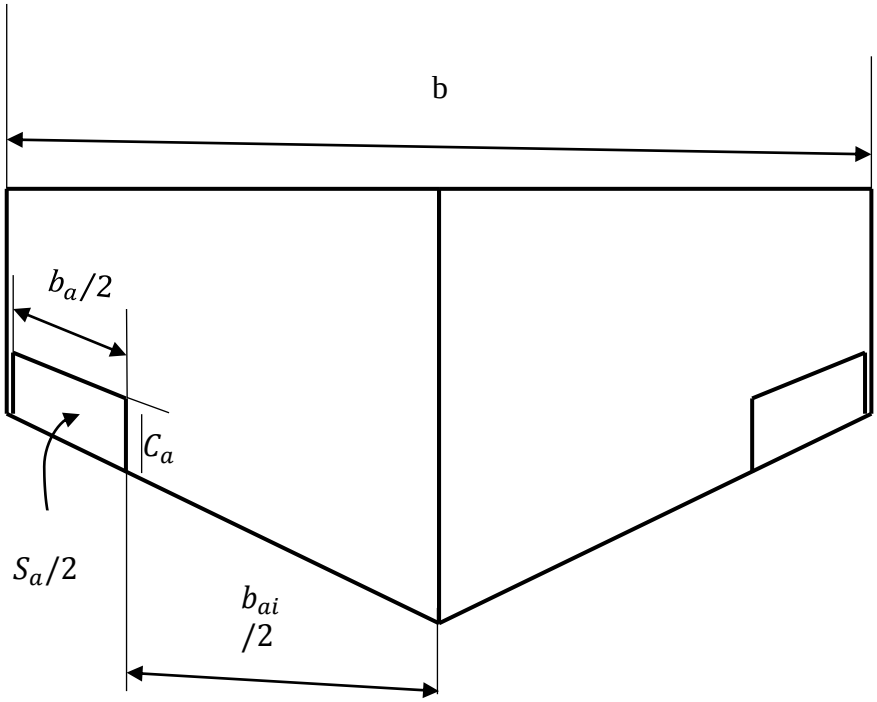

Figure 15: *Aileron layout.*

Raymer [2] provides a graph to estimate the aileron area. Sadraey [3] lists these two parameters for a number of aircrafts which closely match with the graph. The following table lists the characteristics of aileron for Munal M-72.

Table 5: *Aileron Design Parameters.*

b	Span Ratio		Chord Ratio	Area Ratio	Amax	
	b_{ai}/b	b_a/b	C_a/C	S_a/S	Up	Down
2000	0.694	0.302	0.28	0.06998	20	15

Elevator and Rudder Geometry

The span of elevator was made to match the span of the horizontal stabilizer so that the resulting chord length of elevator would be $34\ mm$, which is 30.9% of the total chord length. Similarly, the rudder was made 35% of the area of the vertical stabilizer with span as that of the vertical stabilizer.

Final Configuration

Orthographic view of the Munal M- 27 is shown below.

Page 12-30 © MAT Journals 2020. All Rights Reserved

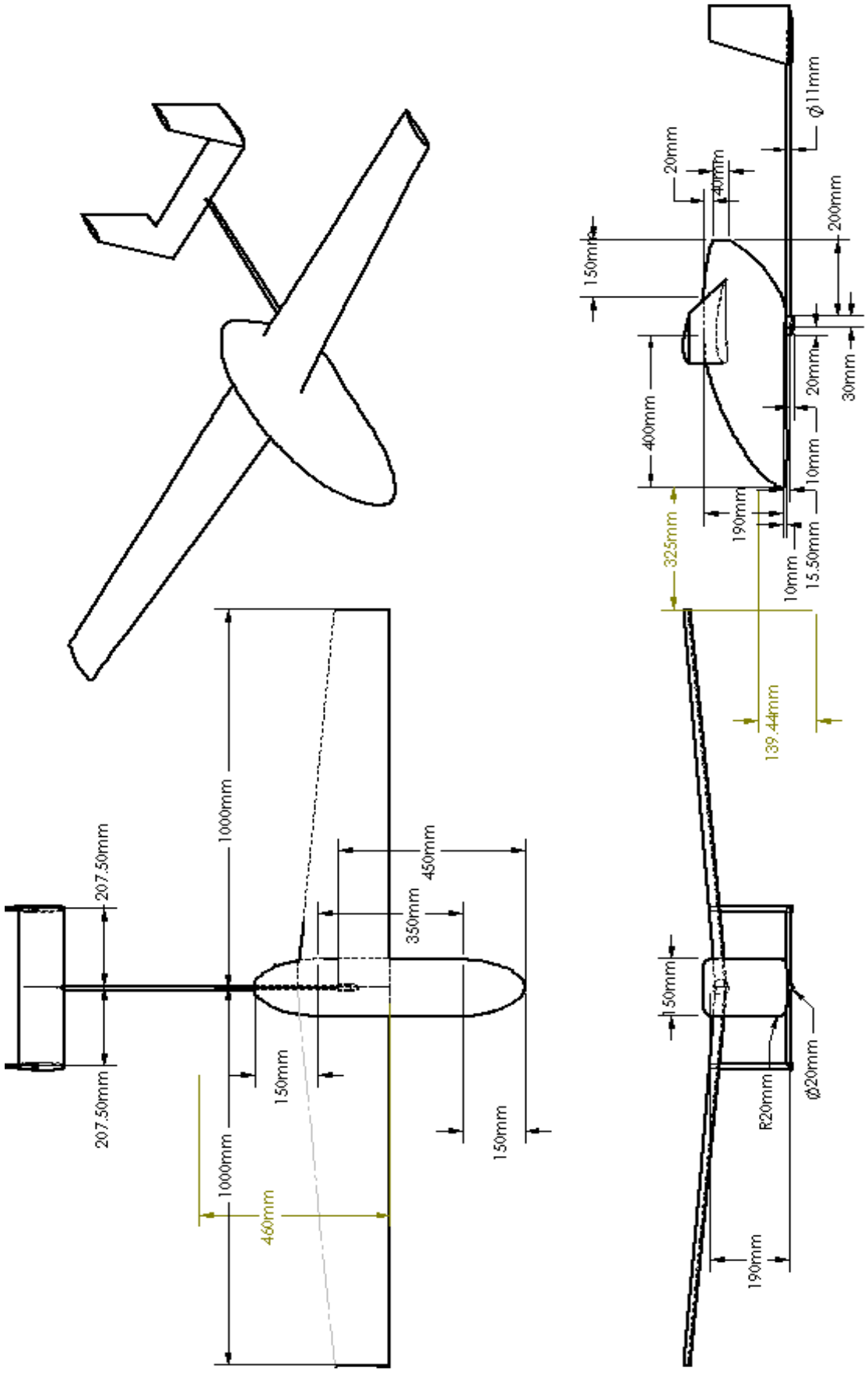

Figure 16: *Orthographic projection of the whole UAV*

Page 12-30 © MAT Journals 2020. All Rights Reserved

AERODYNAMIC ANALYSIS

Munal M-72 was first analyzed using XFLR5. The analysis was done at constant lift, and in the analysis, the contribution of the fuselage was not considered. This analysis was done to obtain the cruising velocity of the UAV so that analysis could be done using ANSYS Fluent. From the analysis, velocity was found to be 15.96 m/s.

In setup, density and viscosity of air were defined as $1.225\ kg/m^3$ and $1.7894e-05\ kg/m^3$ respectively. Inlet velocity was defined and standard atmospheric pressure($101\ kPa$) was used at the outlet. Laminar model was used in the analysis. In this analysis, the main concern was with the lift and drag forces on different parts of the UAV. Total lift and drag forces were found to be 34.58 N and 2.12 N respectively.

Forces - Direction Vector (0 1 0)

Zone	Forces (n) Pressure	Viscous	Total
fuselage	1.2820001	-0.00027222562	1.2817279
wing	16.914902	0.00076159845	16.915664
horizontal_stablizer	-0.92529328	-1.3711014e-05	-0.92530699
vertical_stablizer	0.022628035	-0.00027403133	0.022354004
Net	17.294237	0.00020163049	17.294438

Forces - Direction Vector (0 0 1)

Zone	Forces (n) Pressure	Viscous	Total
fuselage	-0.229433	-0.027028367	-0.25646137
wing	-0.69014366	-0.041005951	-0.73114961
horizontal_stablizer	-0.029957944	-0.0091597229	-0.039117667
vertical_stablizer	-0.024484588	-0.0090409483	-0.033525537
Net	-0.97401919	-0.086234989	-1.0602542

Figure 17: *Lift and drag forces on different components (half portion of the UAV)*

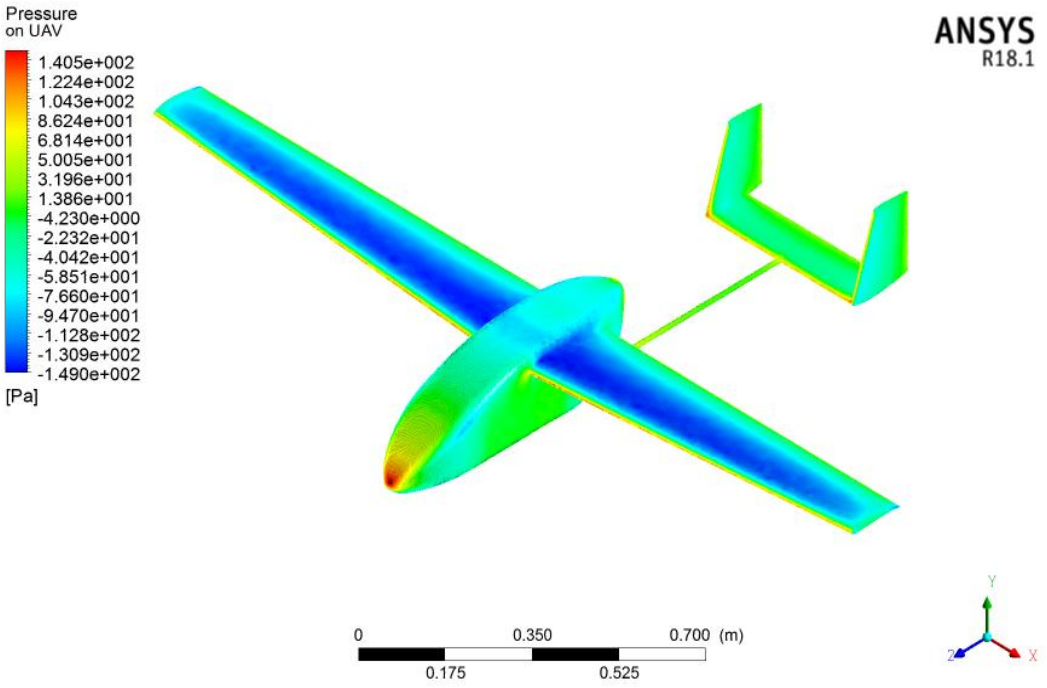

Figure 18: *Pressure Contour.*

Page 12-30 © MAT Journals 2020. All Rights Reserved

STRUCTURAL ANALYSIS

In the final design, the first rib was placed at 7.5% of semi-span from the fuselage centerline, and the remaining span was divided into nine sections using 2 mm thickness ribs. The first rib and rib carrying the servo were thickened to 5 mm for strength. The following CAD model is the geometric model of the half wing of Munal M-72.

Figure 19: *Geometric Model.*

Mechanical and physical properties of the materials that were used in the analysis are presented below:

Table 6: *Material Properties of Elements.*

Material	Property	Value
Carbon Fiber	Tensile Strength (MPa)	2550
	Tensile Modulus (GPa)	135
	Elongation (%)	2.1
	Density (kg/m^3)	1800
	Carbon Content (%)	93
Balsa Wood	Tensile Strength (MPa)	-
	Elastic Modulus (MPa)	3000
	Density (kg/m^3)	160

In reference to the design described, structural analysis was performed. One important criterion of the selection of geometry and material of the component part is deflection. The displacement of the wing tip was to be less than or equal to 5% of the semi-wing span i.e. 50 mm.

Table 7: *Tip Deflection for Different Wing Configuration.*

Design	Material			Maximum Deflection(mm)	
	Front Spar	Rear Spar	Other	LE	TE
1	Balsa	-	Balsa	81.33	86.81
2	Balsa	-	Balsa	80.63	85.28
3	Balsa	-	Balsa	79.51	84.88
4	Balsa	Balsa	Balsa	64.49	67.07
4*	Balsa	Carbon Fiber	Balsa	12.48	12.63

Page 12-30 © MAT Journals 2020. All Rights Reserved

Design 4* is same as design 4 except for the material of the rear spar.
It was observed that the deflection decreased only slightly when the number of ribs was increased from 6 to 16. The 10 ribs were chosen for the final design such that spacing would be convenient for putting skin cover on the wing.

STABILITY

Longitudinal Static Stability

Contribution of different components was considered separately and their contribution were combined in the MATLAB code to check the longitudinal static stability. XFLR5 was used to get the aerodynamic center and moment about the aerodynamic center of the wing, vertical and horizontal stabilizer. Lift curve slope and zero-lift angle of attack were also estimated using XFLR5. Though XFLR5 could be used to check the stability, it was performed manually so that the effect of fuselage in the stability can be analyzed properly.

Zero-lift angle of attack and slope of the coefficient of lift curve for the wing are:
$C_{L\alpha w}$= 0.088 $degree^{-1}$
α_{L0w} = $-6.4\ degree$.

Distance of the aerodynamic center of the wing from the leading edge of root chord (X_{acw}) and moment about the aerodynamic center of wing (M_{acw}) are:
M_{acw} = $-1.64\ Nm$
X_{acw} = 0.04327.

The above relation showed that the aerodynamic center is at 23.5% of mean aerodynamic chord for the wing.

And for horizontal stabilizer,
Slope of the coefficient of lift curve ($C_{L\alpha t}$) = 0.0625 $degree^{-1}$
Aerodynamic center from leading edge of root chord (X_{act}) = 0.0244 m
Moment about aerodynamic center (M_{act}) = 0 (symmetric airfoil)

The fuselage also contributes to the longitudinal stability of aircraft. As the fuselage is cambered, the coefficient of moment about cg due to fuselage at a zero-degree angle for the fuselage reference line (C_{m0f}) and slope of the coefficient of moment ($C_{m\alpha f}$) can be calculated using empirical formulas and graphs as presented by Pamadi [1]. Different points were considered to get the equation of camber line and thickness of the fuselage, and polynomial equations were fitted using Microsoft Excel. For the camber line polynomial equation of 6^{th} order was used, whereas 2^{nd} order equation was used for thickness. The integration was performed for three segments of the fuselage. The integral was calculated using MATLAB.
The result obtained is:
C_{m0f} = -0.0552
$C_{m\alpha f}$ = 0.0026 $degree^{-1}$

In MATLAB, graphs for different default angle of incidence of horizontal stabilizer were plotted. In the program, the distance was measured from the nose of the fuselage. The moment due to drag forces was neglected. For each angle of incidence of the horizontal stabilizer, points with zero moment were found. Then the slope of the coefficient of moment with respect to the angle of attack about the point was calculated.

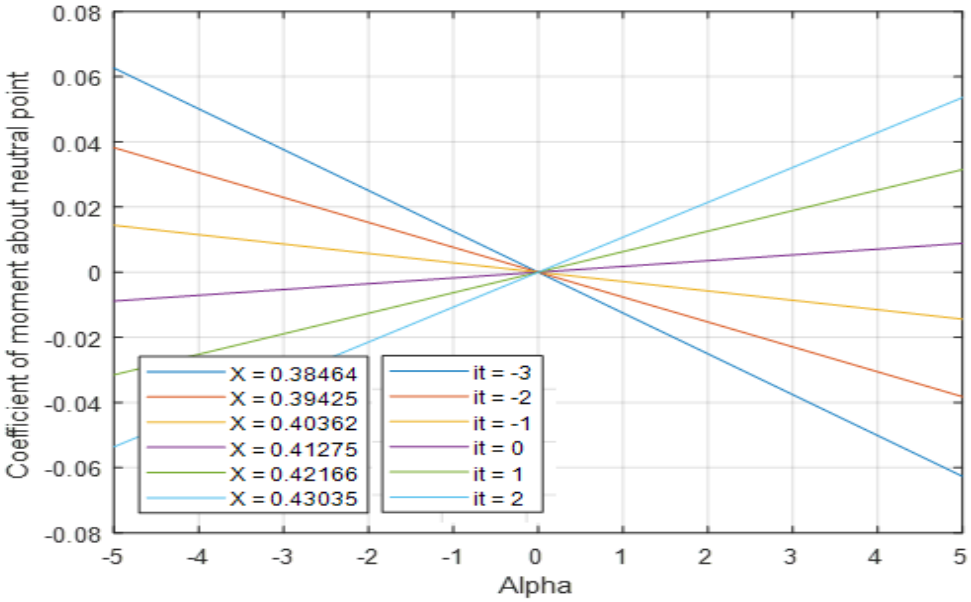

Figure 20: *Coefficient of Moment For Different Angle Of Attack.*

Page 12-30 © MAT Journals 2020. All Rights Reserved

It was decided to keep -2 degrees as the default angle of incidence for the horizontal stabilizer. For the configuration, the cg of the UAV should be located at 0.39425m from the nose of the fuselage.
The mass of the UAV should be arranged as:

Table 8: *Mass, centroid, and positional status of different components*

S.N.	Component	Mass(gram)	Centroid X(mm)	Position status
1.	Fuselage	200.32	368.27	fixed
2.	Wing	180.74	401	fixed
3.	Empennage	114	938.52	fixed
4.	Payload System	2179.14	299.20	variable
5.	Brushless Motor	60	650	fixed
6.	Battery	720	550	variable
7.	Servos (Aileron)	18.32	390.42	fixed
8.	Servo (Horizontal Stabilizer)	9.16	1165	fixed
9.	Servos (Vertical Stabilizer)	18.32	1190	fixed

In the above mass arrangement, the payload system includes both the Payload releasing mechanism and payload. Small components like wires were not considered in the above table.

Directional Static Stability

There is no contribution of the wing to the directional static stability if it does not have a sweep.

The contribution of the fuselage and wing are considered together. Hoak, et al. [4] provides relations for the calculation of the contribution. The slope of the coefficient of yawing moment in sideslip because of wing and fuselage ($C_{n\beta wf}$) was found to be $-0.0003\ degree^{-1}$.
For the contribution of the vertical tail, two units were considered as the single unit. For the single unit,
Slope of the coefficient of lift ($C_{L\alpha v}$) = $0.056\ degree^{-1}$
Mean aerodynamic chord = $0.131\ m$
Area (S_{vt}) = $0.048 m^2$
Aerodynamic center = 22.13% of the mean aerodynamic chord
Distance from cg to the aerodynamic center (L_{vt}) = $0.7447\ m$
It was assumed that the vertical stabilizer experiences same dynamic pressure. Then, the slope of the coefficient of yawing moment with sideslip angle due to the vertical stabilizer ($C_{n\beta v}$) was found to be $0.00278\ degree^{-1}$. The overall slope of the coefficient of yawing moment with sideslip angle ($C_{n\beta}$) was found to be $0.00248\ degree^{-1}$.

Lateral Static Stability

Munal M-72 has a high wing configuration and for the high wing configuration, the slope of the coefficient of rolling moment with sideslip angle ($C_{L'\beta f}$) is $-0.0006\ degree^{-1}$.
In the design of Munal M-72, the vertical stabilizer is placed lower. Further, it was assumed that the center of pressure of the vertical stabilizer was at 40% of the span; then, it would be at $51\ mm$ above the tip of the fuselage. But the center of gravity was around $80\ mm$ above. Thus, the vertical tail has a destabilizing effect on lateral stability.
The slope of the coefficient of rolling moment due to vertical stabilizer ($C_{L'\beta v}$) was found to be $0.000112\ degree^{-1}$. In this calculation, dynamic pressure was assumed to remain same for the vertical stabilizer.
To increase the stability in the lateral direction, it was decided to keep dihedral angle (Γ) of $5\ degrees$. The slope of coefficient of rolling moment due to wing ($C_{L'\beta w}$) was found to be $-0.1\ rad^{-1}$ or $-0.00176\ degree^{-1}$.

Longitudinal Dynamic Stability

To calculate stability derivatives, we used the value of the coefficient of lift and drag of the whole UAV from the numerical analysis done in ANSYS. From that analysis coefficient of lift and drag were found to be 0.6158 and 0.03775 respectively. The moment of inertia about the y-axis passing through cg (I_{YY}) was calculated using SOLIDWORKS and found to be $0.098\ kgm^2$. Based on the above data, stability derivatives were calculated.
$X_u = -0.0379\ s^{-1}$, $Z_u = -1.2383\ s^{-1}$, $M_u = 0$, $X_w = 0.4\ s^{-1}$ (assuming Oswald efficiency factor(e) = 0.9), $Z_w = -5.899\ s^{-1}$, $M_w = -2.99\ m^{-1}s^{-1}$ ($C_{m\alpha} = -0.4526$ per radian), $Z_q = 0$, $X_q = 0$, $M_q = -8.937\ s^{-1}$, $Z_{\dot{w}} = 0$, $M_{\dot{w}} = -0.1615\ m^{-1}$
Then stability matrix is,

$$A = \begin{bmatrix} -0.0379 & 0.4 & 0 & -9.81 \\ -1.2383 & -5.558 & 15.96 & 0 \\ 0.2 & -2.0373 & -11.51 & 0 \\ 0 & 0 & 1 & 0 \end{bmatrix}$$

Using MATLAB, Eigen values of the matrix were found to be -8.5336 $\pm$ 4.8762i and

Page 12-30 © MAT Journals 2020. All Rights Reserved

$-0.0194 \pm 0.6072i$. Using these values, half-life of long period oscillation (LPO) and short period oscillation (SPO) were calculated and found to be 0.0812 s and 35.73 s respectively.

The response of MUNAL M-72 to disturbance of $\Delta u = 0.1u_0 = 1.596\, m/s$ and $\Delta\alpha = 5\ degree$ was plotted in MATLAB.

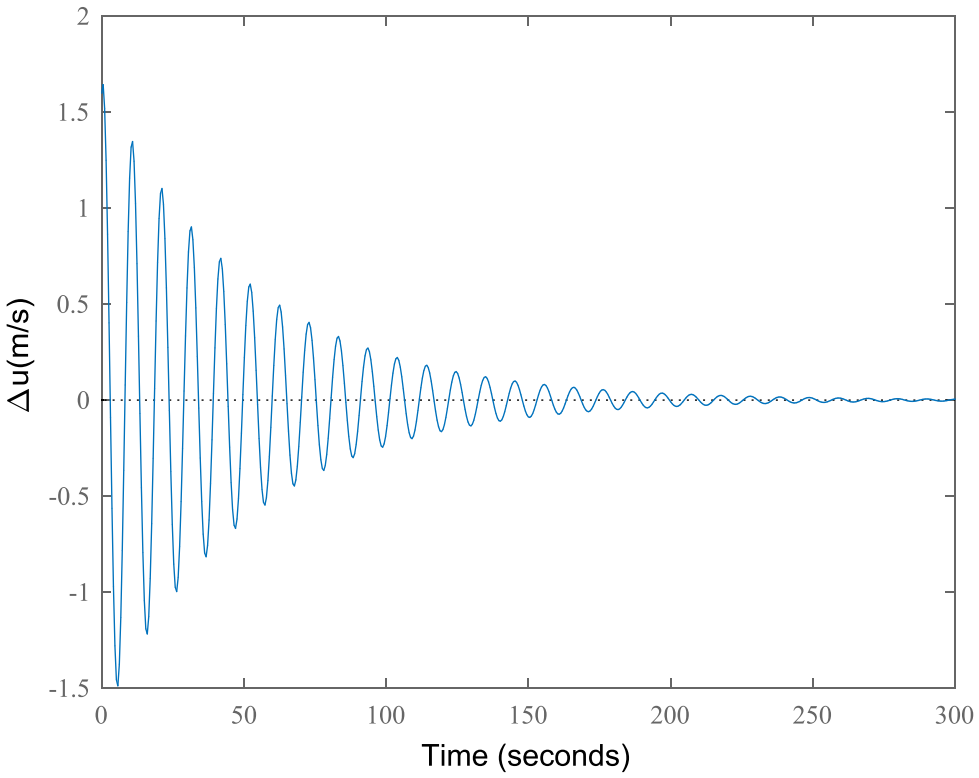

Figure 21: *Response of MUNAL M-72 To Disturbance In ΔU And ΔA – Change In ΔU.*

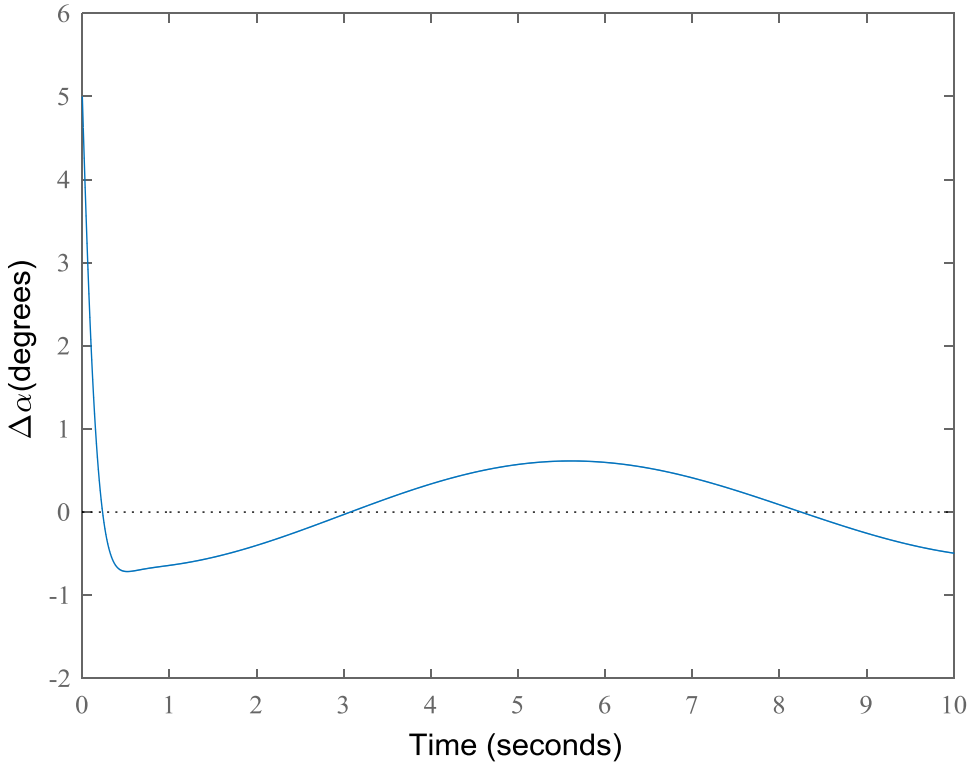

Figure 22: *Response of MUNAL M-72 To Disturbance In ΔU and ΔA – Change In ΔA.*

Page 12-30 © MAT Journals 2020. All Rights Reserved

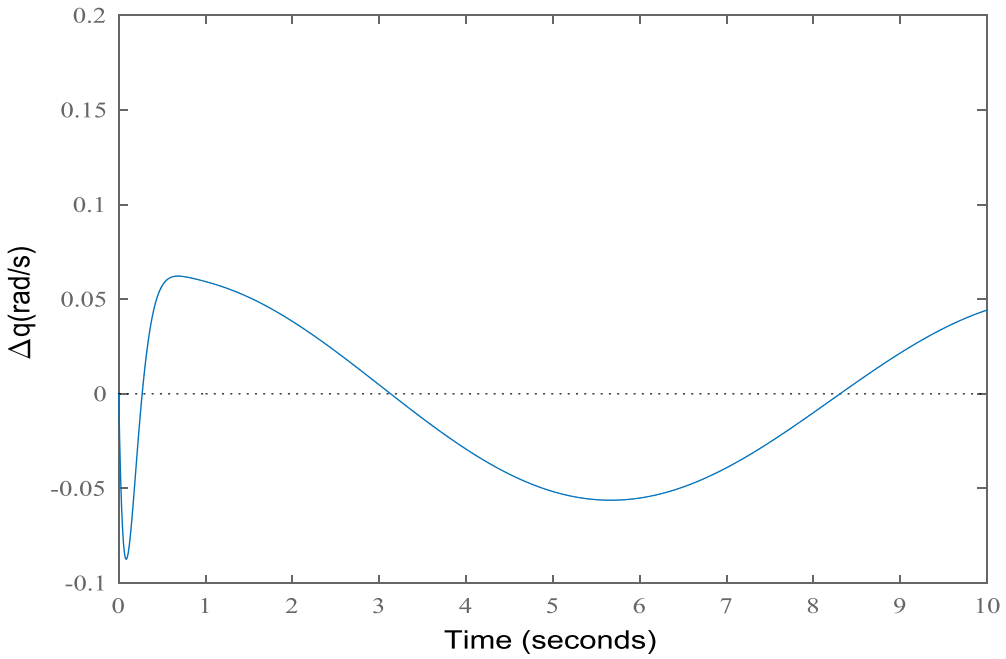

Figure 23: *Response of MUNAL M-72 To Disturbance In ΔU and ΔA – Change In ΔQ.*

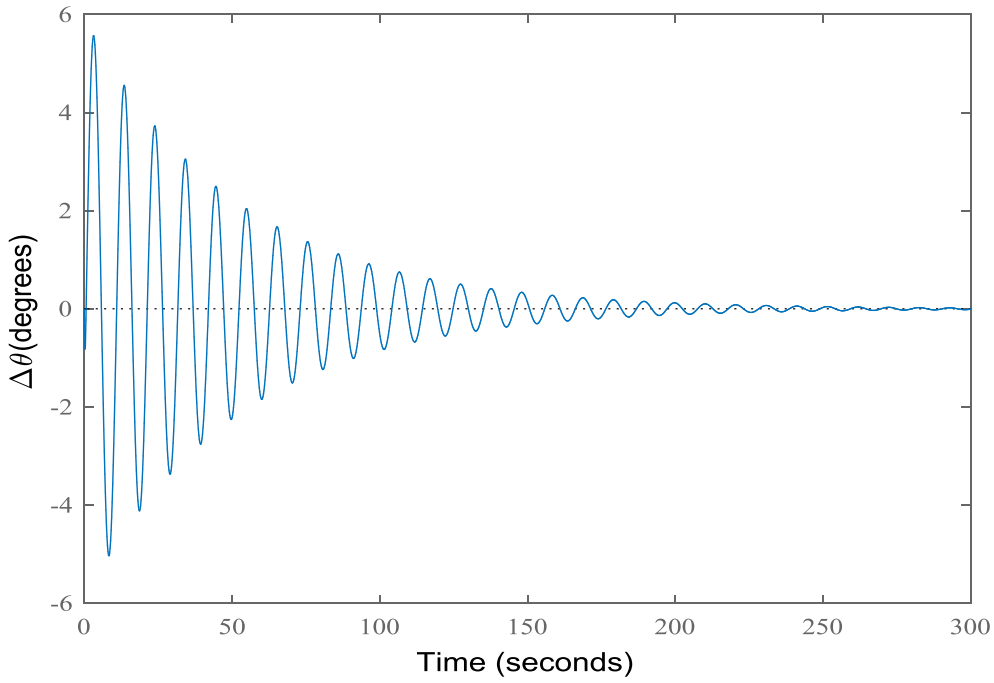

Figure 24: *Response of MUNAL M-72 To Disturbance In ΔU and ΔA – Change In $\Delta \Theta$*

PROPULSION SYSTEM

In level flight, the total thrust should overcome the drag.

$$D = T_{req} = \frac{1}{2} \times \rho \times V^2 \times C_D \times S_{ref}$$

The CFD analysis gave the maximum 3D drag to be approximately $3\ N$.

The cruise speed is set at $15\ m/s$. So, the power required for cruise is given by

$$P_{req.} = Thrust \times Cruise\ speed$$
$$= 45\ Watt$$

A brushless DC motor with higher power rating (40-50% greater) than required in cruise was selected to fly easily at $50 - 60$ % throttle. The additional available power is required during accelerating, climbing and turning flights.

A matching propeller was selected using methods described by Falk [5] and Cook [6].

Page 12-30 © MAT Journals 2020. All Rights Reserved

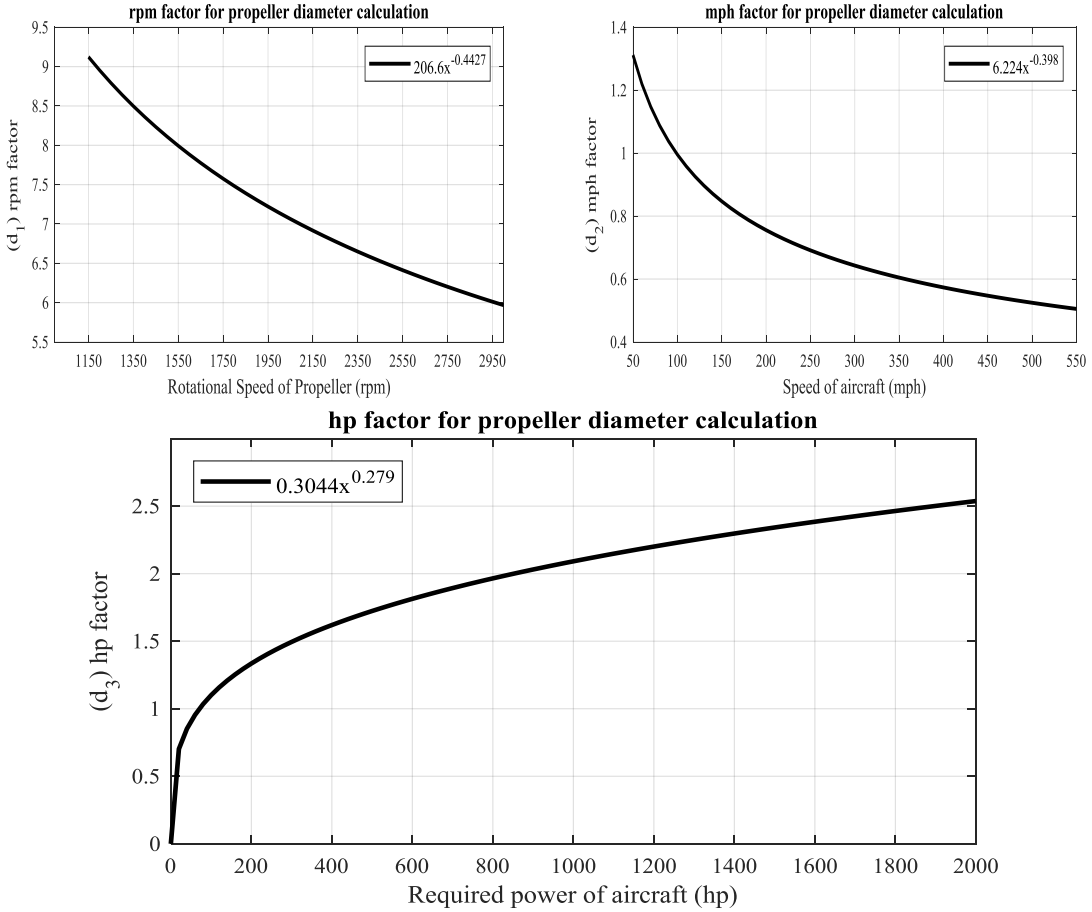

Figure 25: *Extrapolated curves for propeller diameter calculation.*

The following table summarizes the propulsion system components for Munal M-72.

Table 9: *Final Configuration of Propulsion System.*

Motor				
EMAX 1400KV	**KV rating**	**Voltage range**	**Power range**	**Weight**
Brushless Motor	1400 KV	DC 8-12 V	95.2-247.2 W	52 grams
Propeller				
EP 1147 Propeller	Diameter	Pitch	Material	Shaft Diameter
	11 inches	4.7 inches	Plastic	3.2 mm
Battery				
5000 mAh	C-rate	Rated capacity	Size (mm)	Weight
LIPO Battery	25 C	10000 mAh (3s)	36 × 59 × 170	442 grams
ESC				
Sky Walker 40A ESC	BEC	Output Amp.	Burst	Weight
	2A/5V	40 A continuous	40A /10 secs	37 grams

DISCUSSION AND CONCLUSION

Using an iterative design process including aerodynamic, structural and stability analysis, and propulsion selection, a UAV for search and rescue operations is designed. The UAV can be equipped with sensor and payload of around 1 kg and fly for 30 minutes. The UAV will have maximum take-off weight of 3.5 kg and wingspan of 2m. The design can be scaled up for higher payload and endurance capability [7-24].

LIST OF SYMBOLS

W	=	Weight
ρ	=	Density of air
λ	=	Taper ratio
C_l	=	Coefficient of lift for the airfoil
C_L	=	Coefficient of lift for the wing
C_d	=	Coefficient of drag for the airfoil
C_D	=	Coefficient of drag for the wing
α	=	Angle of attack of the aircraft

Page 12-30 © MAT Journals 2020. All Rights Reserved

Re = Reynolds number
$C_{L\alpha w}$ = Slope of the coefficient of lift for the wing
$C_{l\alpha}$ = Slope of the coefficient of lift for the airfoil
A = Aspect ratio
α_{0l} = Zero-lift angle of attack
S_w = Wing referential area
b = Wing span
e = Oswald efficiency number
α_{0lw} = Zero-lift angle of attack for the wing
X_{acw} = Distance of the aerodynamic center of the wing from the leading edge of the root chord
M_{acw} = Moment about the aerodynamic center for the wing
$C_{L\alpha t}$ = Slope of the coefficient of lift for the horizontal stabilizer
X_{act} = Aerodynamic center from the leading edge of the root chord of the horizontal stabilizer
M_{act} = Moment about the aerodynamic center for the horizontal stabilizer
C_{m0f} = Coefficient of moment about cg due to fuselage at zero-degree angle of the fuselage reference line
$C_{m\alpha f}$ = Slope of the coefficient of moment for the fuselage
$C_{n\beta wf}$ = Slope of the coefficient of yawing moment in sideslip because of the wing and fuselage
$C_{L\alpha v}$ = Slope of the coefficient of lift for the vertical stabilizer
S_{vt} = Area of the vertical tail
L_{vt} = Distance from cg to aerodynamic center of the vertical stabilizer
$C_{n\beta v}$ = Coefficient of yawing moment with sideslip angle due to the vertical stabilizer
$C_{n\beta}$ = Yawing moment with sideslip angle
$C_{L'\beta f}$ = Coefficient of rolling moment with sideslip angle due to the fuselage
$C_{L'\beta v}$ = Slope of the coefficient of rolling moment due to the vertical stabilizer
Γ = Dihedral angle
$C_{L'\beta w}$ = Slope of the coefficient of rolling moment due to the wing

REFERENCES

1. Pamadi, B. N. (2004), "Performance, stability, dynamics, and control of airplanes", American Institute of aeronautics and astronautics, Available at https://doi.org/10.2514/4.862274
2. Raymer, D. (2012), "Aircraft design: a conceptual approach", American Institute of Aeronautics and Astronautics, Inc, Available at https://doi.org/10.2514/4.869112
3. Sadraey, M. H. (2012), "Aircraft design: A systems engineering approach", John Wiley & Sons, Available at https://books.google.co.in/books?hl=en&lr=&id=VT-Tc3Tx5aEC&oi=fnd&pg=PT7&dq=Aircraft+design+a+system+engineering+approach&ots=0UMDYUB9sB&sig=9tfM-ZQNDYzfylVaePHkNwpCfaw&redir_esc=y#v=onepage&q=Aircraft%20design%20a%20system%20engineering%20approach&f=false
4. Hoak, D. E., Anderson, R., & Goss, C. R. (1978), "The USAF stability and control DATCOM, Air Force Wright Aeronautical Laboratories", Wright Patterson Air Force Base, Ohio.
5. Falk, K. H. (1944), "Aircraft propeller handbook", New York: Ronald Press.
6. Cook, M. (2007), "Flight dynamics principles: A linear systems approach to aircraft stability", 2nd Edition, 2007, Butterworth-Heinemann, Chapter:" Angular Velocities Transformation.
7. John D. Anderson, J. (2010), "Aircraft Performance and Design", New York: TATA McGraw-Hill.
8. Meredith, P.A. (2011), "An Unmanned Aircraft System for Maritime Search and Rescue", *Stellenbosch University*, Available at http://scholar.sun.ac.za/handle/10019.1/6720
9. Waharte, S., & Trigoni, N. (2010), "Supporting search and rescue operations with UAVs", *2010 International Conference on Emerging Security Technologies* (pp. 142-147). IEEE, Available at https://ieeexplore.ieee.org/abstract/document/5600072
10. Jaeger, M., & Adair, D. (2017), "Conceptual design of a high-endurance hybrid electric unmanned aerial vehicle", *Materials Today: Proceedings*, Volume *4, Issue* 3, pp.4458-4468, Available at https://doi.org/10.1016/j.matpr.2017.04.018
11. Capata, R., Marino, L., & Sciubba, E. (2014), "A hybrid propulsion system for a high-endurance UAV: configuration selection, aerodynamic study,

Page 12-30 © MAT Journals 2020. All Rights Reserved

and gas turbine bench tests", *Journal of Unmanned Vehicle Systems*, Volume *2, Issue* 1, pp.16-35, Available at https://cdnsciencepub.com/doi/full/10.1139/juvs-2013-0005

12. Falk, K. H. (1944), "Aircraft propeller handbook", *New York: Ronald Press.*
13. Cook, M. (2007), "Flight Dynamics Principal", *Butterworth-Heinemann.*
14. "Drone Energy Sources - Pushing the boundaries", (2019), Available at https://www.droneii.com/drone-energy-sources
15. Anderson, J. D. (2012), "Fundamentals of Aerodynamics", *McGraw-Hill*.
16. Caughey, D. A. (2011), "Introduction to Aircraft Stability and Control", *New York.*
17. Russell, J. (1996), "Performance and Stability of Aircraft", *Butterworth-Heinemann*, Available at https://courses.cit.cornell.edu/mae5070/Caughey_2011_04.pdf
18. Valavanis, K. P., & Vachtsevanos, G. J. (Eds.). (2015), "*Handbook of unmanned aerial vehicles* (Vol. 1). Dordrecht: Springer Netherlands.
19. Abbott, G. F. (1986). Propellers. Model Aviation, 12, 6th ser., 42-136. Retrieved May 28, 2019, Available from https://library.modelaviation.com/ma/1986/6/1
20. Patel, K. D., Jayaraman, C., & Maurya, S. K. (2015), "Selection of BLDC Motor and Propeller for Autonomous Amphibious Unmanned Aerial Vehicle", WSEAS *Transactions on Systems and Control*, Volume 10, pp.179-185.
21. Chen, M. (2012), "Static thrust measurement for propeller-driven light aircraft", Proceedings of the 2012 International Conference on Computer Application and System Modeling. Atlantis Press, Available at https://doi.org/10.2991/iccasm.2012.165
22. Gerber, M. (2019), "Motor, Propeller, ESC, and Battery Sizing Introduction", Available at http://www.maclab.seas.ucla.edu/people/matt-gerber/
23. Kiwi, D. (Ed.). (2019), "Welcome to FlyBrushless.com", Available at http://www.flybrushless.com/
24. Staples, G. (1970), "Propeller Static & Dynamic Thrust Calculation - Part 1 of 2", Retrieved May 2, 2019, Available from https://www.electricrcaircraftguy.com/2013/09/propeller-static-dynamic-thrust-equation.html

Page 12-30 © MAT Journals 2020. All Rights Reserved